198522: orthopyroxene–garnet–cordierite pelitic gneiss, Tregenza Road

(Youanmi Terrane, Yilgarn Craton)

Blereau, ER, Korhonen, FJ, Fielding, IOH and Kelsey, DE

Location and sampling

Corrigin (SI 50-3), Brookton (2333)

MGA Zone 50, 538023E 6442092N

Warox Site FJKBGD198522

Sampled on 2 June 2010

This sample was collected from a dam wall in a paddock, about 8.0 km south of Bugin Rock, 7.6 km southwest of Juropin Rock, and 0.2 km north of Tregenza Road. The sample was collected as part of the Geological Survey of Western Australia's (GSWA) 2003–14 Yilgarn Craton Metamorphic Project, and referred to in that study as sample BG10-10d. The results from this project have not been released by GSWA, although select data have been published in Goscombe et al. (2019).

Geological context

The unit sampled is a granulite-grade pelitic gneiss (Fig. 1) near the western margin of the Youanmi Terrane (Quentin de Gromard et al., 2021). The unit is part of a northwest-trending belt of Archean metasedimentary and gneissic rocks referred to by Wilde (2001) and Bosch et al. (1996) as the Jimperding metamorphic belt. The boundary between the South West and Youanmi Terranes in this area is a major, northwest-trending shear zone system (Quentin de Gromard et al., 2021). A sample of pelitic granofels was also collected from this locality (GSWA 198520). Four quartzite samples, collected between 99 and 111 km northwest of this locality, yielded detrital zircon ages between c. 3700 and 3000 Ma, and maximum ages of deposition between c. 3203 and 3005 Ma (GSWA 177901, Wingate et al., 2008a; GSWA 177904, Wingate et al., 2008b; GSWA 177907, Wingate et al., 2008c; GSWA 177908, Wingate et al., 2008d; Pidgeon et al., 2010). Zircon rims in two of these samples have been interpreted to date amphibolite facies metamorphism at c. 2660 Ma (GSWA 177907, Wingate et al., 2008c; GSWA 177908, Wingate et al., 2008d). Monazite from a pelitic gneiss about 21 km to the west-southwest yielded a weighted mean $^{207}Pb/^{206}Pb$ date of 2647 ± 5 Ma, interpreted as the age of high-grade metamorphism (GSWA 198516, Fielding et al., 2021c). Monazite from the sample reported here yielded a weighted mean $^{207}Pb/^{206}Pb$ date of 2656 ± 6 Ma, interpreted as the age of high-grade metamorphism (GSWA 198522, Fielding et al, 2021b). The second sample collected from this locality yielded a similar monazite age of 2651 ± 6 Ma (GSWA 198520, Fielding et al, 2021a), and peak *P–T* estimates of 4.9 – 9.7 kbar and 830–1000 °C (Blereau et al., 2022). A summary of the metamorphic evolution of the southwest Yilgarn Craton is provided in Korhonen et al. (2021).

Petrographic description

The sample is a weakly foliated, medium-grained Fe-rich pelitic gneiss containing about 31% biotite, 26% orthopyroxene, 20% plagioclase, 15% garnet, 4% cordierite, 3% quartz and trace amounts of K-feldspar, ilmenite, monazite and zircon (Fig. 2, Table 1). Biotite occurs as large anhedral laths up to 4 mm in diameter primarily around orthopyroxene, garnet and plagioclase, as well as inclusions in garnet and orthopyroxene (Figs 2, 3). Orthopyroxene is Al-rich (up to 6.3 wt % Al_2O_3, Table 2) and forms large anhedral and elongate grains up to 4 mm in diameter and contains inclusions of biotite, ilmenite, plagioclase and quartz (Fig. 3a,b). Plagioclase occurs as subhedral grains up to 1 mm in diameter that may be weakly sericitized. Garnet forms clusters of anhedral porphyroblasts up to 4.5 mm in diameter that host rounded inclusions of biotite, cordierite, quartz, ilmenite, and orthopyroxene (Figs 2, 3a,c,d). Garnet porphyroblasts are unzoned in Mn, but show a slight increase in Fe and Ca, and slight decrease in Mg contents from core to

rim (Table 2). Cordierite occurs as irregular grains up to 4 mm in diameter (Fig. 2) with partial pinitisation, as intergrowths with quartz (Fig. 3a), and as small rounded inclusions in garnet (Fig. 3c,d). Quartz occurs as small anhedral grains up to 0.5 mm in diameter intergrown with cordierite, biotite, and plagioclase. Ilmenite only occurs as inclusions within orthopyroxene and garnet and at the margins of orthopyroxene. Rare myrmekite is present within the sample. This granulite-facies gneiss was likely derived from a Fe-rich pelitic sedimentary protolith.

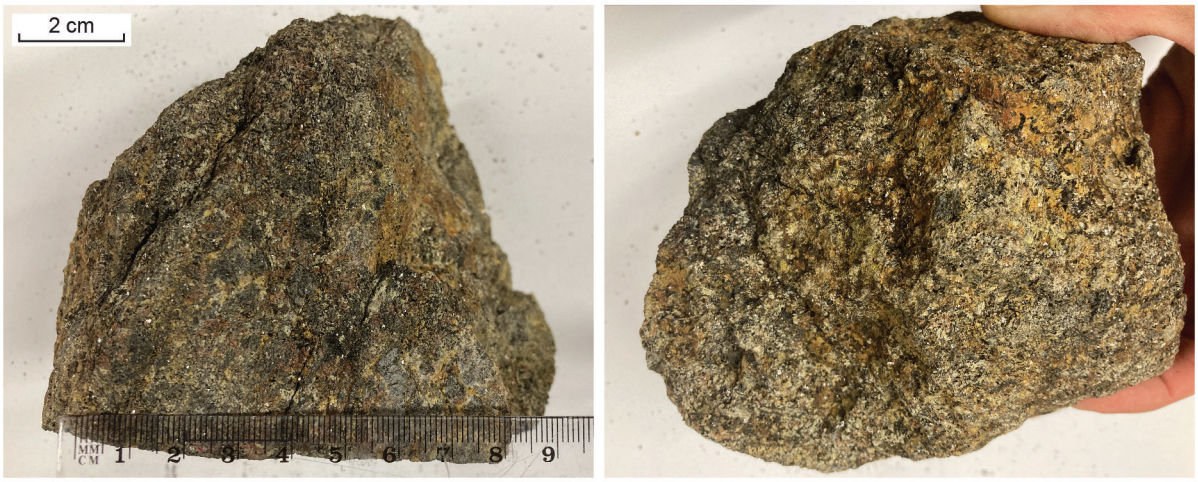

Figure 1. **Hand specimen image of sample 198522: orthopyroxene–garnet–cordierite pelitic gneiss, Tregenza Road**

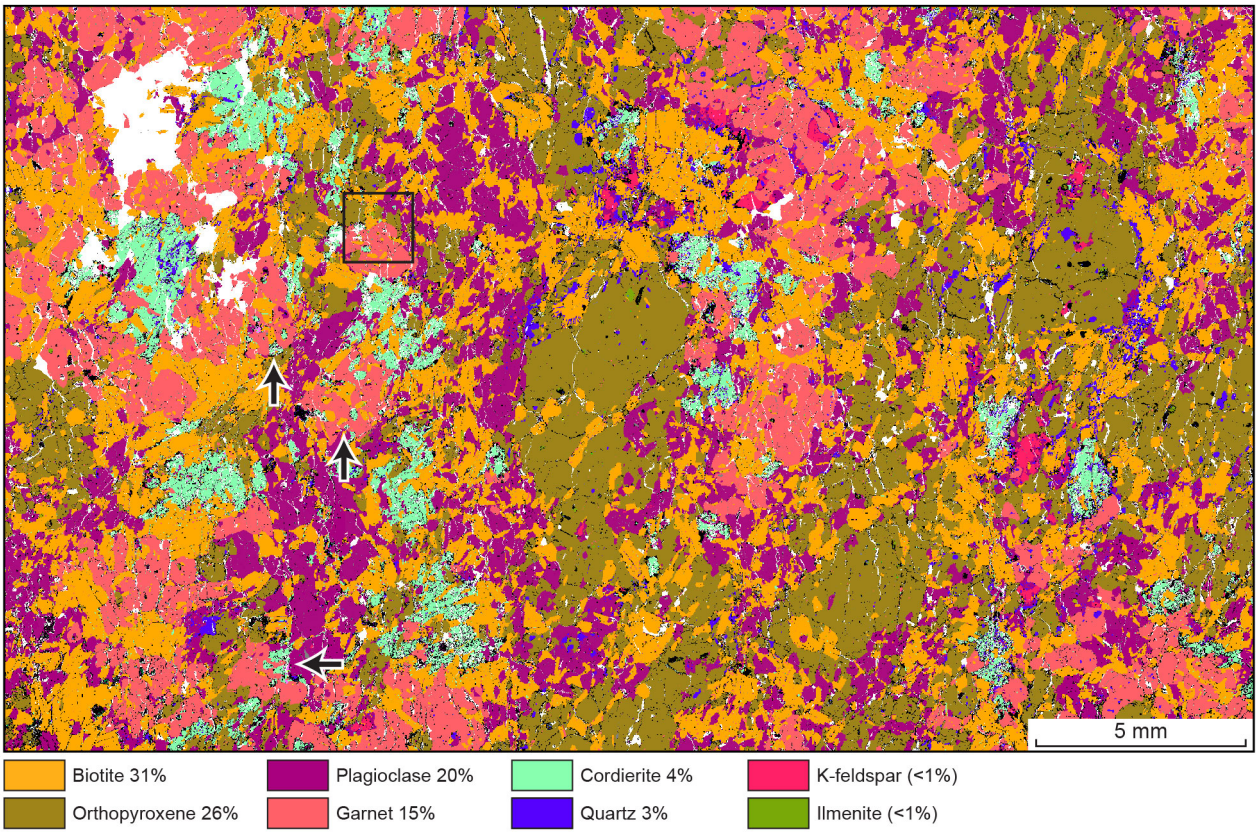

Figure 2. **TESCAN Integrated Mineral Analyser (TIMA) image of an entire thin section from sample 198522: orthopyroxene–garnet–cordierite pelitic gneiss, Tregenza Road. Volume percent proportions of major rock-forming minerals are calculated by the TIMA software. Black box shows area of Figure 3c,d to show cordierite inclusions in garnet. Black arrows outlined in white show other garnet porphyroblasts with cordierite inclusions**

Table 1. Mineral modes for sample 198522: orthopyroxene–garnet–cordierite pelitic gneiss, Tregenza Road

Mineral modes	*Grt*	*Crd*	*Opx*	*Bt*	*Kfs*	*Pl*	*Qz*	*Ilm*	*Mag*	*Liq*
Observed (vol%)	15	4	26	31	trace	20	4	trace	–	–
Predicted (mol%)										
@ 6.2 kbar, 847 °C	28	2	21	17	3	14	6	3	–	6
@ 6.2 kbar, 852 °C	24	3	28	8	9	9	<1	3	–	13
@ 6.0 kbar, 848 °C	20	6	31	9	9	10	<1	3	–	11
@ 5.65 kbar, 837 °C	15	8	26	21	0.7	18	7	2	0.8	–

NOTES: – not present

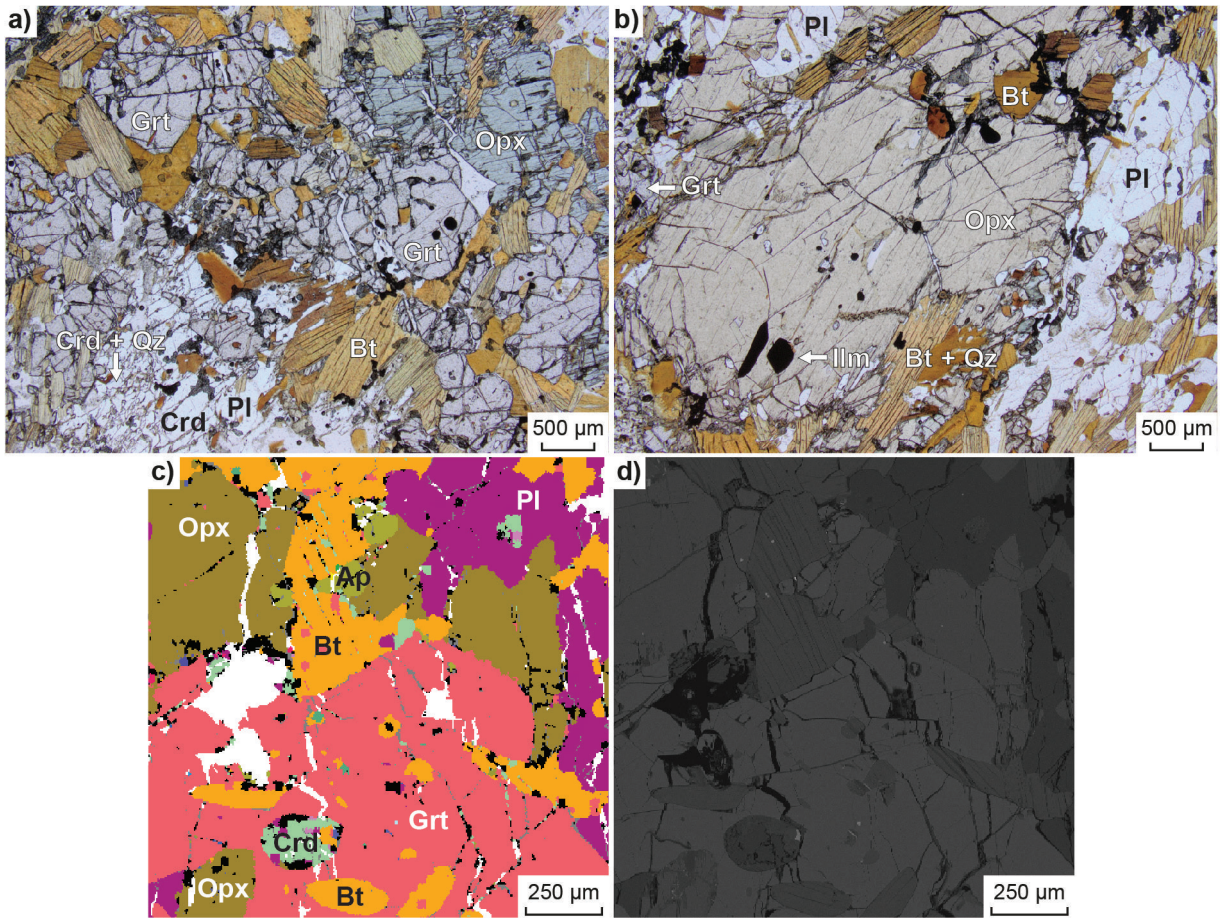

Figure 3. **Thin section images of sample 198522: orthopyroxene–garnet–cordierite pelitic gneiss, Tregenza Road: a,b) photomicrographs in plane-polarized light; c) TIMA image of garnet with inclusions of cordierite, biotite and orthopyroxene (grain location shown on Figure 2); d) backscattered electron image of (c). Mineral abbreviations are explained in the caption to Figure 4, except for Ap, apatite**

Table 2. Mineral compositions for sample 198522: orthopyroxene–garnet–cordierite pelitic gneiss, Tregenza Road

Mineral[(a)]	*Kfs*	*Kfs*	*Pl*	*Pl*	*Grt*	*Grt*	*Grt*	*Bt*	*Bt*	*Bt*	*Opx*	*Opx*	*Opx*	*Ilm*	*Bt*	*Bt*	*Crd*	*Crd*	*Crd*
Setting[(b)]	*Core*	*Rim*	*Core*	*Rim*	*Core*	*Rim*	*OR*	*nOpxC*	*nOpxR*	*nOpxC*	*Core*	*Mantle*	*Rim*	*Core*	*nCrdC*	*nCrdR*	*Core*	*Mantle*	*Rim*
wt%																			
SiO_2	64.88	64.62	61.91	62.02	38.37	39.19	38.45	35.77	35.57	34.73	48.76	48.94	49.11	0.00	36.20	36.04	49.85	49.60	49.09
TiO_2	0.04	0.02	0.01	0.04	0.02	0.03	0.05	5.74	5.76	5.69	0.12	0.11	0.09	47.00	6.24	5.96	0.00	0.02	0.00
Al_2O_3	18.41	18.79	24.75	24.39	21.81	21.75	21.80	14.72	14.96	14.63	6.10	6.31	5.94	0.00	15.04	15.18	32.81	32.79	32.71
Cr_2O_3	0.00	0.00	0.00	0.01	0.02	0.01	0.00	0.04	0.05	0.05	0.00	0.01	0.00	0.06	0.04	0.05	0.01	0.03	0.00
FeO	0.03	0.05	0.09	0.07	27.20	27.66	27.96	15.10	14.97	15.15	24.27	24.67	25.06	46.95	15.28	14.92	5.45	5.16	5.28
MnO	0.00	0.00	0.00	0.00	1.95	2.03	1.90	0.03	0.08	0.09	0.57	0.56	0.60	2.68	0.03	0.04	0.13	0.09	0.10
MgO	0.01	0.01	0.00	0.00	9.12	8.77	8.63	11.97	11.92	11.50	19.49	19.51	19.41	0.04	12.83	12.05	10.64	10.70	10.65
ZnO	0.03	0.00	0.02	0.00	0.07	0.13	0.04	0.14	0.02	0.04	0.00	0.05	0.00	0.03	0.00	0.00	0.00	0.00	0.10
CaO	0.15	0.25	5.79	5.80	0.88	0.95	1.04	0.17	0.06	0.17	0.08	0.08	0.11	0.01	0.00	0.03	0.02	0.01	0.03
Na_2O	1.22	1.64	8.31	8.52	0.01	0.00	0.00	0.25	0.26	0.40	0.04	0.02	0.00	0.05	0.17	0.15	0.20	0.12	0.16
K_2O	14.73	14.69	0.31	0.20	0.00	0.02	0.02	7.29	7.26	6.93	0.00	0.01	0.00	0.01	8.99	7.66	0.02	0.00	0.02
Total[(c)]	99.50	100.07	101.18	101.05	99.47	100.54	99.89	91.20	90.91	89.39	99.42	100.27	100.33	96.83	94.83	92.08	99.14	98.52	98.13
Oxygen	8	8	8	8	12	12	12	11	11	11	6	6	6	3	11	11	18	18	18
Si	3.00	2.96	2.72	2.72	2.98	3.02	2.98	2.77	2.76	2.75	1.84	1.83	1.84	0.00	2.72	2.76	5.01	5.01	4.98
Ti	0.00	0.00	0.00	0.00	0.00	0.00	0.00	0.33	0.34	0.34	0.00	0.00	0.00	0.92	0.35	0.34	0.00	0.00	0.00
Al	1.00	1.02	1.28	1.26	1.99	1.97	1.99	1.34	1.37	1.36	0.27	0.28	0.26	0.00	1.33	1.37	3.88	3.90	3.91
Cr	0.00	0.00	0.00	0.00	0.00	0.00	0.00	0.00	0.00	0.00	0.00	0.00	0.00	0.00	0.00	0.00	0.00	0.00	0.00
Fe^{3+}[(d)]	0.00	0.00	0.00	0.00	0.05	0.00	0.04	0.05	0.05	0.05	0.05	0.05	0.05	0.17	0.05	0.05	0.14	0.09	0.17
Fe^{2+}	0.00	0.00	0.00	0.00	1.71	1.78	1.77	0.93	0.92	0.95	0.72	0.72	0.73	0.85	0.91	0.91	0.32	0.34	0.28
Mn^{2+}	0.00	0.00	0.00	0.00	0.13	0.13	0.12	0.00	0.01	0.01	0.02	0.02	0.02	0.06	0.00	0.00	0.01	0.01	0.01
Mg	0.00	0.00	0.00	0.00	1.06	1.01	1.00	1.38	1.38	1.36	1.10	1.09	1.08	0.00	1.44	1.37	1.59	1.61	1.61
Zn	0.00	0.00	0.00	0.00	0.00	0.01	0.00	0.01	0.00	0.00	0.00	0.00	0.00	0.00	0.00	0.00	0.00	0.00	0.01
Ca	0.01	0.01	0.27	0.27	0.07	0.08	0.09	0.01	0.01	0.01	0.00	0.00	0.00	0.00	0.00	0.00	0.00	0.00	0.00
Na	0.11	0.15	0.71	0.73	0.00	0.00	0.00	0.04	0.04	0.06	0.00	0.00	0.00	0.00	0.02	0.02	0.04	0.02	0.03
K	0.87	0.86	0.02	0.01	0.00	0.00	0.00	0.72	0.72	0.70	0.00	0.00	0.00	0.00	0.86	0.75	0.00	0.00	0.00
Total	5.00	5.00	5.00	5.00	8.00	8.00	8.00	7.60	7.59	7.61	4.00	4.00	4.00	2.00	7.71	7.59	11.00	11.00	11.00
Compositional variables																			
y(Opx)[(e)]	–	–	–	–	–	–	–	–	–	–	0.11	0.11	0.10	–	–	–	–	–	–

NOTES: – not applicable
(a) Mineral abbreviations explained in the caption to Figure 4
(b) OR, outer rim; nXXC, near mineral XX core; nXXR, near mineral XX rim
(c) Totals on anhydrous basis
(d) Fe^{3+} contents for biotite assumed to be 10% of Fe total; Fe^{3+} contents for other minerals based on Droop (1987)
(e) *y*(Opx) = Al on the M1 site; White et al. (2014a)

Analytical details

Preliminary *P–T* estimates were obtained using multiple-reaction thermobarometry calculated from the mineral compositions (Table 2; Goscombe et al., 2019). These estimates were derived from the 'averagePT' module (avPT) in the program THERMOCALC version tc325 (Powell and Holland, 1988), using the internally consistent Holland and Powell (1998) dataset.

The metamorphic evolution of this sample has subsequently been re-evaluated using phase equilibria modelling, based on the bulk-rock composition (Table 3). The bulk-rock composition was determined by X-ray fluorescence spectroscopy, together with loss on ignition (LOI). FeO content was analysed by Fe^{2+} titration, and Fe_2O_3 calculated by difference. The modelled O content (for Fe^{3+}) was reduced slightly (= 21% Fe^{3+} of total Fe) from the titration value (26% Fe^{3+}), in order to reduce the stability of magnetite that is predicted for more oxidized bulk compositions. The H_2O content based on the measured LOI amount is too high and did not allow for prediction of the interpreted peak mineral assemblage. Exploration with calculated phase equilibria at different hydration states prior to calculation of the *P–T* pseudosection constrained a slightly drier hydration state as being suitable for use as the amount of H_2O. The bulk composition was also adjusted for the presence of apatite by applying a correction to CaO (Table 3). Thermodynamic calculations were performed in the MnNCKFMASHTO ($MnO–Na_2O–CaO–K_2O–FeO–MgO–Al_2O_3–SiO_2–H_2O–TiO_2–O$) system using THERMOCALC version tc340 (updated October 2013; Powell and Holland, 1988) and the internally consistent thermodynamic dataset of Holland and Powell (2011; dataset tc-ds62, created in February 2012). The activity–composition relations used in the modelling are detailed in White et al. (2014a,b). Additional information on the workflow with relevant background and methodology are provided in Korhonen et al. (2020).

Table 3. Measured whole-rock and modelled compositions for sample 198522: orthopyroxene–garnet–cordierite pelitic gneiss, Tregenza Road

XRF whole-rock composition (wt%)[a]												
SiO_2	**TiO_2**	**Al_2O_3**	**Fe_2O_3**	**FeO**	**MnO**	**MgO**	**CaO**	**Na_2O**	**K_2O**	**P_2O_5**	**LOI**	**Total**
47.30	1.61	15.14	4.76	12.2[b]	0.41	11.00	1.17	1.38	2.47	0.20	1.00	98.64
Normalized composition used for phase equilibria modelling (mol%)												
SiO_2	**TiO_2**	**Al_2O_3**	**O[c]**	**FeO^{T}[d]**	**MnO**	**MgO**	**CaO[e]**	**Na_2O**	**K_2O**	**–**	**H_2O[f]**	**Total**
49.38	1.26	9.31	1.49	14.37	0.36	17.12	1.00	1.40	1.64	–	2.66	100

NOTES: (a) Data and analytical details are available from the WACHEM database <http://geochem.dmp.wa.gov.au/geochem/>
(b) FeO analysed by Fe^{2+} titration; Fe_2O_3 content calculated by difference
(c) O content (for Fe_2O_3) adjusted
(d) FeO^T = moles FeO + 2 * moles O. Also modified to remove pyrrhotite = moles FeO^T - moles SO_2
(e) CaO modified to remove apatite: CaO(Mod) = CaO(Total) - (moles CaO(in Ap) = 3.33 * moles P_2O_5)
(f) H_2O content based on $T–M_{H2O}$ diagram; see text for additional details

Results

Metamorphic *P–T* estimates have been derived based on detailed examination of one thin section and the bulk-rock composition; care was taken to ensure that the thin section and the sample volume selected for whole-rock chemistry were similar in terms of featuring the same minerals in approximately the same abundances (Table 1), to minimize any potential compositional differences. The *P–T* pseudosection was calculated over a *P–T* range of 4–8 kbar and 750–900 °C (Fig. 4). The solidus is located between 805 and 835 °C across the range of modelled pressures. Cordierite is stable below 6.5 kbar across the range of modelled temperatures, with garnet absent at pressures below 4.8 kbar at 830 °C and 5 kbar at 900 °C. Quartz is absent at temperatures above the solidus, with a minimum temperature stability of 820 °C at 4 kbar, extending to higher temperatures with increasing pressure. Orthopyroxene is stable over the range of modelled conditions. Magnetite is stable with cordierite-bearing assemblages at pressures below 6.2 kbar across the range of modelled temperatures, and spinel is stable at pressures below 5.8 and temperatures above 885 °C.

Metamorphic *P–T* estimates (± 2σ uncertainty) calculated using multiple-reaction thermobarometry are 6.1 ± 0.6 kbar and 814 ± 29 °C (Goscombe et al., 2019). These calculations used the mineral core compositions (Table 2) to estimate peak conditions.

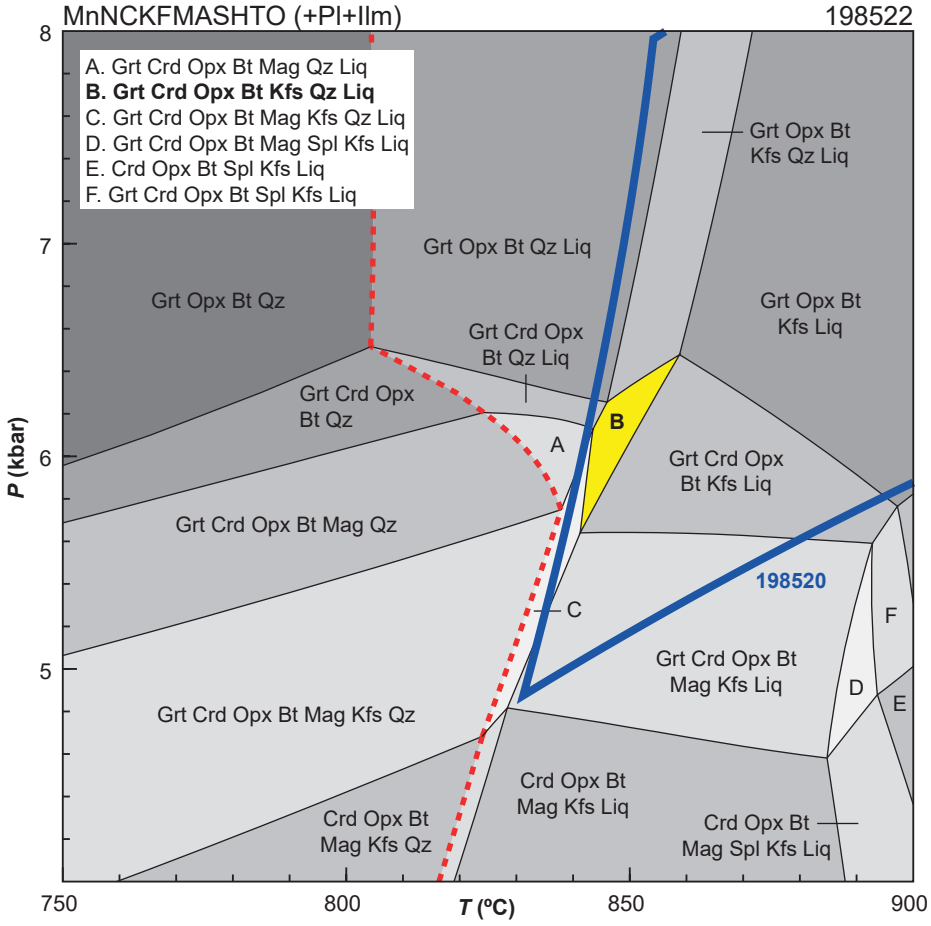

Figure 4. ***P–T*** **pseudosection calculated for sample 198522: orthopyroxene–garnet–cordierite pelitic gneiss, Tregenza Road. Assemblage field corresponding to peak metamorphic conditions is shown in bold text and yellow shading. Red dashed line represents the solidus. Blue field corresponds to peak *P–T* estimates from a sample collected from the same locality (GSWA 198520). Thick blue lines show the region of overlap between the two samples, which is the best estimate for peak conditions. Abbreviations: Bt, biotite; Crd, cordierite; Grt, garnet; Ilm, ilmenite; Kfs, K-feldspar; Liq, silicate melt; Mag, magnetite; Opx, orthopyroxene; Pl, plagioclase; Qz, quartz; Spl, spinel**

Interpretation

Based on the coarse grain size and mineral associations that support textural equilibrium, the peak granulite-grade metamorphic assemblage is interpreted to be garnet–cordierite–orthopyroxene–biotite–K-feldspar–quartz–plagioclase–ilmenite–melt. Some of the coarse-grained biotite around orthopyroxene and garnet is interpreted to be retrograde. Inclusions of orthopyroxene and cordierite are preserved in garnet (Figs 2, 3c,d), suggesting that the growth of these minerals may have pre-dated at least some garnet growth, although the possibility that these inclusion minerals were in equilibrium with the garnet host cannot be ruled out.

The inferred peak assemblage of garnet–cordierite–orthopyroxene–biotite–K-feldspar–quartz–plagioclase–ilmenite–melt is stable between 845 and 860 °C at 5.6 – 6.5 kbar. The predicted mineral modes (molar proportions approximately equivalent to vol%) across the peak field are broadly similar to the modes observed in the thin section (Table 1). However, the observed modes most closely match the predicted modes in the garnet–cordierite–orthopyroxene–biotite–magnetite–K-feldspar–quartz–plagioclase–ilmenite field at conditions just below the solidus (Table 1), although magnetite is not observed in the sample. Some retrograde growth of biotite following melt crystallization accounts for a higher abundance of observed biotite as compared to predicted modes at the solidus. The inferred sequence of mineral growth of orthopyroxene and cordierite, followed by garnet growth at the expense of these minerals is consistent with an anticlockwise *P–T* path.

Peak metamorphic conditions are estimated at 845–860 °C and 5.6 – 6.5 kbar. The other sample collected from the same locality yields peak *P–T* estimates of 4.9 – 9.7 kbar and 830–1000 °C (GSWA 198520, Blereau et al., 2022). The peak assemblage field of the sample reported here occurs within these *P–T* constraints (Fig. 4). These estimates are just slightly higher than the results of multiple-reaction thermobarometry (Goscombe et al., 2019), although do overlap if uncertainties related to the thermodynamic modelling are propagated.

Based on the results of two samples from the same locality, peak metamorphic conditions are estimated at 5.6 – 6.5 kbar and 845–860 °C, with an apparent thermal gradient of approximately 130–150 °C/kbar. The growth of garnet at the expense of orthopyroxene and cordierite broadly supports an anticlockwise *P–T* path.

References

Blereau, ER, Korhonen, FJ, Kelsey, DE and Fielding, IOH 2022, 198520: garnet-bearing orthopyroxene pelitic granofels, Tregenza Road; Metamorphic History Record 14: Geological Survey of Western Australia, 10p.

Bosch, D, Bruguier, O and Pidgeon, RT 1996, Evolution of an Archean metamorphic belt: A conventional and SHRIMP U–Pb study of accessory minerals from the Jimperding metamorphic belt, Yilgarn Craton, Western Australia: The Journal of Geology, v. 104, p. 695–711.

Droop, GTR 1987, A general equation for estimating Fe3+ concentrations in ferromagnesian silicates and oxides from microprobe analyses, using stoichiometric criteria: Mineralogical Magazine, v. 51, no. 361, p. 431–435.

Fielding, IOH, Wingate, MTD, Korhonen, FJ and Rankenburg, K 2021a, 198520: pelitic granofels, Tregenza Road; Geochronology Record 1765: Geological Survey of Western Australia, 5p.

Fielding, IOH, Wingate, MTD, Korhonen, FJ and Rankenburg, K, 2021b; 198522: pelitic granofels, Tregenza Road; Geochron Record 1766: Geological Survey of Western Australia, 5p.

Fielding, IOH, Wingate, MTD, Korhonen, FJ and Rankenburg, K 2021c, 198516: pelitic granofels, Quajabin Peak; Geochronology Record 1764: Geological Survey of Western Australia, 5p.

Goscombe, B, Foster, DA, Blewett, R, Czarnota, K, Wade, B, Groenewald, B and Gray, D 2019, Neoarchaean metamorphic evolution of the Yilgarn Craton: a record of subduction, accretion, extension and lithospheric delamination: Precambrian Research, article no. 105441, doi:10.1016/j.precamres.2019.105441.

Holland, TJB and Powell, R 2011, An improved and extended internally consistent thermodynamic dataset for phases of petrological interest, involving a new equation of state for solids: Journal of Metamorphic Geology, v. 29, no. 3, p. 333–383.

Korhonen, FJ, Blereau, ER, Kelsey, DE, Fielding, IOH and Romano, SS 2021, Metamorphic evolution of the southwest Yilgarn, *in* Accelerated Geoscience Program extended abstracts: Geological Survey of Western Australia, Record 2021/4, p. 108–115.

Korhonen, FJ, Kelsey, DE, Fielding IOH and Romano, SS 2020, The utility of the metamorphic rock record: constraining the pressure–temperature–time conditions of metamorphism: Geological Survey of Western Australia, Record 2020/14, 24p.

Pidgeon, RT, Wingate, MTD, Bodorkos, S and Nelson, DR 2010, The age distribution of detrital zircons in quartzites from the Toodyay – Lake Grace Domain, Western Australia: implications for the early evolution of the Yilgarn Craton: American Journal of Science, v. 310, p. 1115–1135.

Powell, R and Holland, TJB 1988, An internally consistent dataset with uncertainties and correlations: 3. Applications to geobarometry, worked examples and a computer program: Journal of Metamorphic Geology, v. 6, no. 2, p. 173–204.

Quentin de Gromard, R, Ivanic, TJ and Zibra, I 2021, Pre-Mesozoic interpreted bedrock geology of the southwest Yilgarn, 2021, in Accelerated Geoscience Program extended abstracts: Geological Survey of Western Australia, Record 2021/4, p. 122–144.

White, RW, Powell, R, Holland, TJB, Johnson, TE and Green, ECR 2014a, New mineral activity-composition relations for thermodynamic calculations in metapelitic systems: Journal of Metamorphic Geology, v. 32, no. 3, p. 261–286.

White, RW, Powell, R and Johnson, TE 2014b, The effect of Mn on mineral stability in metapelites revisited: New a–x relations for manganese-bearing minerals: Journal of Metamorphic Geology, doi:10.1111/jmg.12095.

Wilde, SA 2001, Jimperding and Chittering metamorphic belts, Western Australia — a field guide: Geological Survey of Western Australia, Record 2001/12, 24p.

Wingate, MTD, Bodorkos, S, and Kirkland, CL 2008a, 177901: quartzite, Kowalyou; Geochronology Record 739: Geological Survey of Western Australia, 5p.

Wingate, MTD, Bodorkos, S, and Kirkland, CL 2008b, 177904: quartzite, Windmill Hill; Geochronology Record 740: Geological Survey of Western Australia, 7p.

Wingate, MTD, Bodorkos, S, and Kirkland, CL 2008c, 177907: quartzite, Noondeening Hill; Geochronology Record 741: Geological Survey of Western Australia, 7p.

Wingate, MTD, Bodorkos, S, and Kirkland, CL 2008d, 177908: quartzite, Noondeening Hill; Geochronology Record 742: Geological Survey of Western Australia, 7p.

Links

Metamorphic history introduction document: Intro_2020.pdf

Recommended reference for this publication

Blereau, ER, Korhonen, FJ, Fielding, IOH and Kelsey DE 2022, 198522: orthopyroxene–garnet–cordierite pelitic gneiss, Tregenza Road; Metamorphic History Record 15: Geological Survey of Western Australia, 8p.

Data obtained: 19 May 2020

Date released: 14 April 2022

This Metamorphic History Record was last modified on 29 March 2022.

Grid references in this publication refer to the Geocentric Datum of Australia 1994 (GDA94). All locations are quoted to at least the nearest 100 m.

WAROX is GSWA's field observation and sample database. WAROX site IDs have the format 'ABCXXXnnnnnnSS', where ABC = geologist username, XXX = project or map code, nnnnnn = 6 digit site number, and SS = optional alphabetic suffix (maximum 2 characters).

Isotope and element analyses are routinely conducted using the GeoHistory laser ablation ICP-MS and Sensitive High-Resolution Ion Microprobe (SHRIMP) ion microprobe facilities at the John de Laeter Centre (JdLC), Curtin University, with the financial support of the Australian Research Council and AuScope National Collaborative Research Infrastructure Strategy (NCRIS). The TESCAN Integrated Mineral Analyser (TIMA) instrument was funded by a grant from the Australian Research Council (LE140100150) and is operated by the JdLC with the support of the Geological Survey of Western Australia, The University of Western Australia (UWA) and Murdoch University. Mineral analyses are routinely obtained using the electron probe microanalyser (EPMA) facilities at the Centre for Microscopy, Characterisation and Analysis at UWA, and at Adelaide Microscopy, University of Adelaide.

Digital data related to WA Geology Online, including geochronology and digital geology, are available online at the Department's Data and Software Centre and may be viewed in map context at GeoVIEW.WA.

Further details of geoscience products are available from:
Information Centre
Department of Mines, Industry Regulation and Safety
100 Plain Street
EAST PERTH WA 6004
Telephone: +61 8 9222 3459 | Email: publications@dmirs.wa.gov.au
www.dmirs.wa.gov.au/GSWApublications